Thermodynamics of the Ce γ–α transition: Density-functional study

Y. Wang,[1] L. G. Hector, Jr.,[2] H. Zhang,[1] S. L. Shang,[1] L. Q. Chen,[1] and Z. K. Liu[1]
[1]*Materials Science and Engineering, The Pennsylvania State University, University Park, Pennsylvania 16802, USA*
[2]*GM R&D Center, 30500 Mound Road, Warren, Michigan 48090, USA*
(Received 15 July 2008; revised manuscript received 21 August 2008; published 19 September 2008)

We investigate the Cerium γ–α isostructural phase transition by explicitly incorporating finite temperature mixing of the Ce nonmagnetic and magnetic states. Unique to our approach is the calculation of vibrational properties from phonon theory. The critical behavior of the transition is shown to be controlled by the configurational mixing entropy between the magnetic and nonmagnetic states. Our theoretical framework leads to accurate predictions of the critical point and equation of state associated with the Ce γ–α phase transition.

DOI: 10.1103/PhysRevB.78.104113 PACS number(s): 64.70.−p, 05.70.Jk, 63.20.dk, 05.70.Ce

I. INTRODUCTION

Cerium (Ce, atomic number 58) was identified in 1803 and named in honor of Ceres, the largest known "planetesimal" in the asteroid belt.[1] As the first of the rare earth (or lanthanide) series elements with f electrons, and by far the most abundant of this series in the earth's crust (~0.0046%), Ce displays intriguing physical and chemical properties of which the most fascinating is its first-order isostructural phase transition, discovered by P.W. Bridgman in 1927.[2,3] This involves a magnetic, high-temperature/high-volume "γ phase" and a nonmagnetic, low-temperature/low-volume "α phase." At 298 K and 0.7 GPa, the $\gamma \rightarrow \alpha$ transition is accompanied by a 14%–17% volume collapse leaving the crystal structure unchanged as face-centered cubic (fcc).

The Ce phase transition has been the subject of extensive debate as evidenced in the numerous theoretical models[4–16] that have appeared in the intervening decades since its discovery. Some early theoretical studies focused on key aspects of the physics of the transition. For example, Zachariasen and Pauling (see references in Johansson *et al.*[8]) suggested that the transition results from 4f electron promotion into the 5d-6s valence band; Allen and Martin[4] proposed a Kondo volume collapse due to a change in the conduction screening of the localized 4f electron; and a Mott transition, by which the 4f electron is localized in γ-Ce but itinerant in α-Ce, was advocated by Johansson.[17] Some more recent studies focused on phase transition thermodynamics and/or application of density functional theory (DFT) to predict important thermodynamic quantities, such as the critical point or volume collapse. For example, Wang[11] presented a classical mean-field potential study of Ce but did not reproduce the critical point. Lüders *et al.*[15] and Amadon *et al.*[16] emphasized the important role of entropy[8,9] in the $\gamma \rightarrow \alpha$ transition, although vibrational entropy was not included. Free energy as a function of temperature was computed by Lüders *et al.*[15] with the self-interaction corrected local spin density approximation (SIC-LSD). Amadon *et al.*[16] used the local density approximation (LDA) and dynamical mean-field theory (LDA-DMFT) to predict Ce energetics as a function of temperature. In contrast to the earlier result of Held *et al.*,[12] who with a different implementation of LDA-DMFT demonstrated an emerging double well below T=0.136 eV (~1600 K), Amadon *et al.*[16] found no double tangent in their predicted energy vs volume relation.

Despite the important insights that existing theoretical models of the Ce transition have provided, considerable uncertainty remains due to the wide range of predicted thermodynamic properties[5,8–10,15] relative to published experimental data.[3,18–23] This is likely due, in part, to various assumptions or omissions in existing theoretical models, such as LDA overbinding, or the lack of a concise formulation for the free energy of Ce. Such a formulation must include the electronic energy, lattice vibrations, and the configurational mixing entropy among the different electronic states.

Motivated by the need for a theoretical approach that accurately predicts key thermodynamic quantities of the Ce phase transition, we formulate the Helmholtz free energy in terms of a partition function that allows for finite temperature mixing of Ce nonmagnetic and magnetic electronic states. All partition function inputs are computed from DFT,[24] as implemented in the Vienna *ab initio* simulation package (VASP)[30–32] accounting for strong correlation of the Ce f states. Specifically, we incorporate electronic and vibrational contributions from both nonmagnetic and magnetic Ce 4f states, and account for the statistical average over the two electronic states through an appropriate range of volumes and temperatures. Phonon spectra, from which vibrational contributions are taken, are computed with the direct method to lattice dynamics and compared to published experimental data. We explore the double well structure and miscibility gap (or two phase region) in the free energy and compare our predicted values of the critical point, phase transition temperature at ambient pressure, and $\gamma \rightarrow \alpha$ volume collapse with experiments. We also investigate additional thermodynamic quantities and the fraction of nonmagnetic and magnetic Ce along the phase boundary, the T-V phase diagram, and the equation of states.

The remainder of this paper is organized as follows. In Sec. II, we describe our thermodynamic model of the Ce γ–α phase transition. Our computational approach, which involves DFT and phonon calculations, is detailed in Sec. III. Section IV provides a comparison of key thermodynamic properties from the present and previous theoretical models with experiments. Computed phonon spectra for nonmagnetic and magnetic Ce are examined in Sec. V. In Sec. VI, we explore the entropy and the vibrational entropy change and the role of configurational entropy in the transition. Also examined are selected thermodynamic terms and the fraction of magnetic Ce along the phase boundary, the T-V phase dia-

gram, and the equation of states. Key results are summarized in Sec. VII.

II. THERMODYNAMIC MODEL

It has long been believed that the γ–α phase transition is due to competition between Ce electronic states,[4,8,17] as suggested by previous studies of the volume collapse, equation of states (EOS), and critical point.[3,18,23,25] The Helmholtz free energy must therefore account for finite temperature configurational mixing of the different electronic states. For this purpose, we can first assume that the thermodynamic fluctuations happen locally (i.e., atom by atom) following the pseudoalloy model.[8,9,15] A partition function, Z, which assumes a canonical ensemble, where the atomic volume (V) and temperature (T) are constants, is then written as[26,27]

$$Z = \sum_{\sigma} Z^{\sigma} = \sum_{\sigma} \exp[-\beta F^{\sigma}(V,T)]. \quad (1)$$

Note that σ in Eq. (1) labels the local electronic state, $F^{\sigma}(V,T)$ is the Helmholtz free energy for σ, $Z^{\sigma}=\exp[-\beta F^{\sigma}(V,T)]$ is the partition function for σ, and $\beta=1/k_BT$. Summation over σ in Eq. (1) addresses the statistical average over different local electronic states, while remaining statistical degrees of freedom have been incorporated into $F^{\sigma}(V,T)$. For Ce, the summation over σ in Eq. (1) includes both the nonmagnetic electronic state (i.e., the local spin moment is zero) and the magnetic electronic state (i.e., the local spin moment is not zero).

Equation (1) connects the Helmholtz free energy[27] $F(V,T)=-k_BT \log Z$ for a system with many electronic states to that of an individual electronic state σ via $F^{\sigma}(V,T)=-k_BT \log Z^{\sigma}$. Hence,

$$F(V,T) = -k_BT\sum_{\sigma} x^{\sigma} \log Z^{\sigma} + k_BT\left[\sum_{\sigma} x^{\sigma} \log Z^{\sigma} - x^{\sigma} \log Z\right]$$

$$= \sum_{\sigma} x^{\sigma}F^{\sigma}(V,T) - TS_{\text{conf}}. \quad (2)$$

The configurational mixing entropy, S_{conf}, which is an immediate result of Eq. (1), is

$$S_{\text{conf}} = -k_B\sum_{\sigma} x^{\sigma} \log x^{\sigma}. \quad (3)$$

An additional result of Eq. (1) is that $x^{\sigma}=Z^{\sigma}/Z$ is the probability for finding electronic state σ in the system under constant V and T.

To evaluate $F^{\sigma}(V,T)$, we write[11]

$$F^{\sigma}(V,T) = E_c^{\sigma}(V) + F_{\nu}^{\sigma}(V,T) + F_{\text{mag}}^{\sigma}(V,T) + F_{\text{el}}^{\sigma}(V,T), \quad (4)$$

where E_c^{σ} is the 0 K total (static) energy. Remaining terms in Eq. (4) are the vibrational free energy, F_{ν}^{σ}; the magnetic free energy, F_{mag}^{σ}; and the thermal electronic free energy associated with electronic excitation at finite temperatures, F_{el}^{σ}.

III. COMPUTATIONAL APPROACH

Density functional theory as implemented in VASP[28–30] was used to evaluate Eq. (4). The Ce potential was of the projector-augmented wave (PAW)-type[31,32] with a $5s^25p^64f5d6s^2$ valence configuration. The exchange-correlation part of the density functional was treated within the generalized gradient approximation (GGA) of Perdew-Burke-Ernzerhof (PBE) in conjunction with the interpolation formula of Vosko *et al.*[28,33] Calculations on the single-atom Ce primitive cells (both nonmagnetic and ferromagnetic) were conducted with a $20\times20\times20$ Γ-centered k mesh consisting of 256 symmetry-unique k points. In all cases the total energy was converged to 10^{-7} eV/unit cell with a 500-eV plane wave cutoff energy.

Phonon spectra were computed with the direct approach to lattice dynamics[34,35] with VASP as the computational engine. This approach is based upon the calculation of total energies and forces for the equilibrium geometry and several distorted structures resulting from small atomic displacements. Fourier transformation of the resulting force constants yields the dynamical matrix, diagonalization of which provides phonon frequencies and eigenvalues for each selected q point in reciprocal space. Integration over a large sample of q vectors in the entire Brillouin zone yields the phonon density of states from which thermodynamic functions such as the vibrational free energy and entropy are computed. The merits of the direct method used in the present paper relative to other approaches to lattice dynamics have been detailed elsewhere.[36,37] For all phonon calculations, atomic displacements of ±0.02 Å were applied to $2\times2\times2$ (32 Ce atom) supercells. The supercell size was chosen such that interactions between equivalent atoms in periodic images were negligible, as were the computed force constants at the boundaries of each supercell. Extensive tests with larger displacements and supercells revealed no significant differences from the chosen settings. Three supercells were required for each phonon calculation as dictated by the $Fm\bar{3}m$ space group of the nonmagnetic and magnetic Ce structures. Reciprocal space integration was performed by means of the Methfessel-Paxton technique[38] with a 0.2-eV broadening. The phonon results showed no sensitivity to small deviations in smearing width above and below 0.2 eV. Additional computational details associated with the direct approach may be found in Ref. 39.

Evaluation of Eq. (4) for Ce[13,40,41] is problematic in the absence of strong correlation of the f electrons in the DFT Hamiltonian. The relative stability of the nonmagnetic ("delocalized") Ce $4f$ state to that of the magnetic ("localized") Ce $4f$ state is greatly overestimated in the GGA with spin polarization. We surmount this with the Dudarev DFT+U method,[42] implemented in VASP,[29] for both nonmagnetic and magnetic electronic states in Ce. Here the on-site Coulomb and exchange interactions as described with a Hartree-Fock approximation are added to the DFT Hamiltonian.[43] This method offers the advantage that only the difference between the Hubbard U (due to the energy increase from an electron addition to a specific site) and the J (due to the screened exchange energy) need be specified *a priori*.

Evaluation of numerous $U-J$ values over a 1.0–6.0-eV range revealed that 1.6 eV gives the most consistent prediction of nonmagnetic Ce and magnetic Ce energetics over the range of atomic volumes that includes both phases. Alterna-

TABLE I. Theoretical and experimental data associated with the Ce $\gamma \rightarrow \alpha$ transition. T_0: transition temperature at 0 GPa; V_N: atomic volume at room temperature and pressure (i.e., normal conditions); P_c: critical pressure; T_c: critical temperature; V_c: Ce atomic volume at the critical point; P_t: transition pressure associated with $\gamma \rightarrow \alpha$ volume collapse at room temperature (300 K); V_γ: equilibrium atomic volume of "γ phase" at P_t; V_α: equilibrium atomic volume of "α phase" at P_t; $V_\gamma - V_\alpha$: volume collapse at 300 K.

	Present theory	Previous theories	Experiments
T_0(K)	165	135,[a] 169[b]	141 ± 10 [c]
V_N (300 K, 0 GPa) (Å^3)	33.74	37.31,[a] 32.67,[d]31.1,[e] 29.9[b]	34.367[c]
P_c (GPa)	2.22	3.86,[a] 4.7,[d] 0.88,[e] 5.6,[b] 1.3[f]	1.45,[g] 1.75,[h] 1.80,[i] 1.96 ± 0.20 [c]
T_c (K)	476	980,[a]1300,[d] 550,[e] 1377,[b] 520[f]	480,[g] 550,[h] 485,[i] 600 ± 50 [c]
V_c (Å^3)	28.58	25.6,[d] 28.5,[e] 31.1[f]	~29.9,[i] ~29.9 [j]
P_t (300 K) (GPa)	0.87	0.7,[a] 1.0,[d] 0.61,[b] 0.8[f]	0.7 ± 0.06,[c] ~0.9 [i]
V_γ (300 K, $P=P_t$) (Å^3)	32.38	31.6,[d] 30.4,[e] 29.2,[b] 32.8[f]	~32.7,[i] ~33.3 [j]
V_α (300 K, $P=P_t$) (Å^3)	27.02	24.26,[d] 26.7,[e] 23.2,[b] 30.0[f]	~27.9,[i] ~28.3 [j]
$V_\gamma - V_\alpha$ (Å^3)	5.36 (300 K, $P=P_t$)	7.41,[d] 3.7,[e] 6.0,[b] 2.8[f]	~4.8,[i] ~5.0 [j]

[a]Results calculated within GGA by Johansson *et al.* (Ref. 8).
[b]Results calculated within SIC-LSD using Kondo volume-collapse model by Lüders *et al.* (Ref. 15).
[c]Reference 3.
[d]Results calculated within SIC-LSD by Svane (Ref. 9).
[e]Results calculated within SIC-LSD using Kondo volume-collapse model by Lægsgaard and Svane (Ref. 10).
[f]Results of Kondo volume-collapse model with parameters are determined from the experimental data of La and Pr by Allen and Liu (Ref. 5).
[g]Reference 21.
[h]Reference 19.
[i]Reference 23.
[j]Reference 18.

tively, for $U-J=\sim 1.7$ eV, the computed 0-K energy of magnetic Ce is comparable to that of nonmagnetic Ce, which is physically implausible since γ-Ce is not observed at 0 K. Values of $U-J$ larger than 1.7 eV were precluded from consideration since magnetic Ce is lower in energy than nonmagnetic Ce at 0 K. For their work on $Ce_{55}Al_{45}$ metallic glass, Sheng *et al.*[44] used a value of $U-J=5.6$ eV demonstrating the need for care in the choice of $U-J$. Successful applications of the Dudarev *et al.*[42] approach to strong correlation to other materials may be found in Refs. 43, 45, and 46.

Since F_ν^σ requires the total phonon density of states (DOS),[47] we included strong correlation of the f electrons in all DFT calculations.[34,48] While we do not consider quasiparticle renormalization,[12,16] we note that existing theories[12,16] detailing the role of quasiparticle renormalization on the Ce $\gamma \rightarrow \alpha$ transition are controversial. For example, Held *et al.*[12] suggested that the volume collapse is due to the quasiparticle resonance in the $4f$ spectrum (which in turn results in a negative curvature in the energy versus volume curve). However, Amadon *et al.*[16] showed that the magnitude of this stabilization energy is too small to induce a pronounced negative curvature. We also neglect spin-orbit coupling since it will have a very minimal effect on Ce phase transition thermodynamics.

For magnetic Ce, F_{mag}^σ has been approximated by[11]

$$F_{\text{mag}}^\sigma(V,T) = -k_B T \ln[1 + M_S(2l - M_S)], \tag{5}$$

where k_B is Boltzmann's constant, M_S the spin moment, and $l=3$ is the orbital angular momentum of an f electron. Equation (5) is a generalization of Hund's rule, with total angular momentum $J=M_S(2l-M_S)/2$. Note that Eq. (5) leads to values of F_{mag}^σ in good agreement with previous results.[8,9,15] The remaining term in Eq. (4), F_{el}^σ, was evaluated via integration over the electronic DOS following the Fermi-Dirac distribution.[27] Evaluation of Eq. (2) also involved 4$^{\text{th}}$-order polynomial fitting[49] with

$$F(V,T) = a(T) + b(T)V^{-2/3} + c(T)V^{-4/3} + d(T)V^{-6/3} + e(T)V^{-8/3} \tag{6}$$

to extrapolate $F^\sigma(V,T)$ for each electronic state in the instance that the required volume departed from the appropriate volume range for the Ce transition. This extrapolation did not have a significant effect on our results.

IV. THEORY/EXPERIMENT COMPARISONS

Key quantities calculated from our model are compared to previous theoretical work[8–10,15] and available experimental data[3,18,19,21,23] in Table I. These are: T_0 (the 0-GPa transition temperature); V_N (the atomic volume under ambient conditions); P_c (the critical point pressure); T_c (the critical point

temperature); V_c (the Ce volume at the critical point); P_t (the room-temperature transition pressure); V_γ (the γ-Ce equilibrium atomic volume at P_t); and V_α (the α-Ce equilibrium atomic volume at P_t). Of the available critical point measurements, the widely referenced values of T_c=600 K and P_c=2.0 GPa (Refs. 8, 16, 50, and 51) are from Koskenmaki and Gschneidner[3] and Beecroft and Swenson[18] (listed as 1.96 GPa). Alternatively, Kutsar[21] reported T_c=480 K and P_c=1.45 GPa and Schiwek *et al.*[23] recently reported T_c=485 K and P_c=1.8 GPa. These latter T_c values are noticeably lower than those of previous measurements.[18,19]

With the model in Sec. II, we find T_c=476 K and P_c=2.22 GPa. At 300 K, we predict a 5.36 Å^3 $\gamma \rightarrow \alpha$ volume collapse ($V_\gamma - V_\alpha$), which is in excellent agreement with the experimental values[18,23] of ~4.8 Å^3 and ~5.0 Å^3. Experimental P_t values of 0.7 GPa (Ref. 18) and ~0.9 GPa (Ref. 23) bound our predicted 0.87 GPa value.

From the theoretical work of Lüders *et al.*,[15] T_0=169 K, and that from the present theory is 165 K. Both values are in reasonable accord with the 141 ± 10 K experimental value from Koskenmaki and Gschneidner.[3] However, the predicted critical point values of T_c=1377 K and P_c=5.60 GPa in Lüders *et al.* greatly exceed the Koskenmaki and Gschneidner experimental values of 600 K and 2.0 GPa.[3,8,16,50,51] Using the pseudoalloy model with the single-site coherent potential approximation and the GGA, Johansson *et al.*[8] predicted a critical point of T_c=980 K and P_c=3.86 GPa. With the Kondo volume-collapse (KVC) model and inputs from experiments on La and Pr, Allen and Liu[5] reported a critical point of $T_c \sim 520$ K and $P_c \sim 1.3$ GPa. At 300 K, their volume collapse of 2.8 Å^3 is below the reported experimental values[18,23] of ~4.8 Å^3 and ~5.0 Å^3. Using the SIC-LSD approximation (and neglecting phonon contributions), Svane[9] reported a 7.41 Å^3 volume collapse at 300 K, and Lüders *et al.*[15] noted a 6.0 Å^3 volume collapse: both values fall outside the 4.8–5.0 Å^3 range from experiments. Lægsgaard and Svane[10] used the KVC model, together with the self-interaction corrected local density approximation (SIC-LDA) (neglecting phonon contributions), and reported a 300-K volume collapse of 3.7 Å^3, which is below the experimental range.

V. PHONON SPECTRA

A. Phonon DOS

Figure 1 shows the phonon DOS for ferromagnetic Ce (solid red curve) and nonmagnetic Ce (dot-dashed blue curve) calculated at lattice constants of 5.161 Å and 4.840 Å, respectively. Also shown are experimental data for γ-Ce (no comparable data for α-Ce were available), which is paramagnetic (disordered local moments). The open squares represent data from Manley *et al.*[52] and the dashed black line is from Stassis *et al.*[53] The suitability of Dudarev's approach for strong correlation of the Ce f electrons is demonstrated by the close agreement between our calculated vibrational spectra and experiments. Notable differences between the computed phonon DOS for ferromagnetic and nonmagnetic Ce are: (a) the shifting of the shoulder at 1.5 THz (nonmagnetic) to 1.0 THz (ferromagnetic); (b) the shifting and substantial enhancement of the peak at 2.4 THz (nonmagnetic) to 2.14 THz (ferromagnetic); (c) and the substantial shifting of the peak at 3.5 THz (nonmagnetic) to 2.6 THz (ferromagnetic).

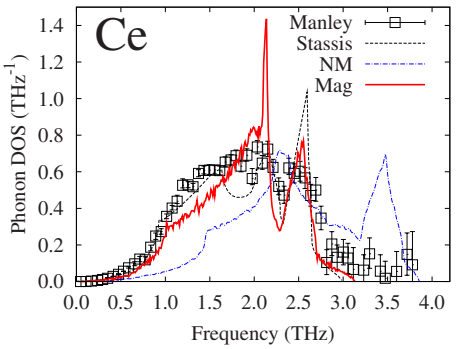

FIG. 1. (Color online). Phonon density of states for Ce. Red (solid) curve: DFT with strong correlation for ferromagnetic (Mag) Ce at a=5.161 Å; blue (dot-dashed) curve: DFT with strong correlation for nonmagnetic (NM) Ce at a=4.84 Å. Black (dashed) curve: from Stassis *et al.* (Ref. 53) calculated using the force constants obtained by fitting the measured phonon dispersions with the Born-von Karman model; □ with error bars are measured phonon density of states for γ-Ce after Manley *et al.* (Ref. 52).

B. Phonon dispersion

Figure 2 shows computed phonon dispersion relations for ferromagnetic Ce (at lattice constant a=5.161 Å, three branches, represented by the solid red curves) and nonmagnetic Ce (a=4.840 Å, three branches, represented by the dot-dashed blue curves), together with experimental data from Stassis *et al.*[53] for γ-Ce (filled circles, paramagnetic with disordered local moments). We note that 5.161 Å is the measured value for γ-Ce at 298 K,[3] and 4.840 Å gives an atomic volume very close to the 28.2 Å^3 experimental value for α-Ce cited by Lüders *et al.*[15] The predicted phonon dispersion of ferromagnetic Ce reproduces the abnormal dip at the "L" point observed for γ-Ce. Alternatively, our calculations for nonmagnetic Ce do not show this abnormal dip.

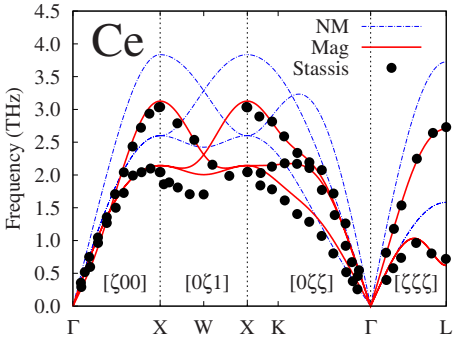

FIG. 2. (Color online). Phonon dispersion relations for Ce. Red (solid) curves, DFT with strong correlation for ferromagnetic (Mag) Ce at a=5.161 Å; blue (dot-dashed) curves, DFT with strong correlation for nonmagnetic (NM) Ce at a=4.840 Å; ●, measured data for γ-Ce from Stassis *et al.* (Ref. 53). The symbol ζ denotes the reduced wave vector (Ref. 53).

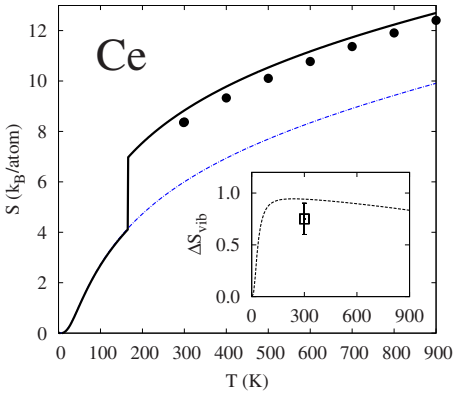

FIG. 3. (Color online). Total entropy, S, and vibrational entropy change, ΔS_{vib}, of Ce at 0 GPa with T(K). The black (solid) and blue (dot-dashed) curves represent, respectively, the calculated entropies for the mixed and nonmagnetic electronic states. ●: Entropy of γ-Ce from the Barin table (Ref. 55). The black (dashed) curve plotted in the inset shows the calculated vibrational entropy change of the magnetic electronic state relative to the nonmagnetic electronic state. □ (open square with error bar in the inset) from Jeong *et al.* (Ref. 25) is their estimated vibrational entropy change at 0.7 GPa of γ-Ce relative to α-Ce.

VI. THERMODYNAMIC PROPERTIES

A. Role of entropy

Although it is commonly believed that the Ce $\gamma \rightarrow \alpha$ transition is entropy driven,[8,9,15,16,54] the role of the vibrational entropy has not been explored in sufficient detail.[52,54] The total entropy, S, may be calculated using Eq. (2) with[27]

$$S(V,T) = -\left(\frac{\partial F(V,T)}{\partial T}\right)_V. \tag{7}$$

Figure 3 shows the calculated entropy, S (k_B/atom), as a function of $T(K)$, computed at V corresponding to $P=0$ GPa. The blue (dot-dashed) and black curves correspond to the nonmagnetic electronic state and mixed state from Eq. (7), respectively. The jump along the black line corresponds to the calculated transition temperature of $T_0=165$ K at 0 GPa. Our calculated total entropy variation with temperature for the mixed state compares favorably with data from the Barin table (filled circles in Fig. 3).[55]

Using the calculated phonon DOS shown in Fig. 1, we have also calculated ΔS_{vib}, the vibrational entropy change of the magnetic electronic state relative to the nonmagnetic electronic state, with increasing T(K) at 0 GPa. The calculated ΔS_{vib} is shown in the inset of Fig. 3 as the black dashed curve, together with an experimentally estimated value by Jeong *et al.*[25] (open square, measured at 300 K corresponding to a transition pressure of 0.7 GPa). Our calculated ΔS_{vib} of $\sim 0.94\ k_B$ is in favorable accord with the $0.75 \pm 0.15\ k_B$ value of Jeong *et al.*[25]

Our calculated total entropy change of 2.86 k_B, corresponding to the jump in the black curve at 165 K in Fig. 3, is approximately 1.3 k_B higher than the experimentally estimated value of 1.54 k_B.[3] This overestimate can be tracked back to Eq. (5) which gives a magnetic entropy $\sim 1.92\ k_B$. This is similar to the value of 1.79 k_B ($k_B \log 6$) from Johansson *et al.*[8] and Svane[9] or 2.08 k_B ($k_B \log 8$) from Lüders *et al.*[15]

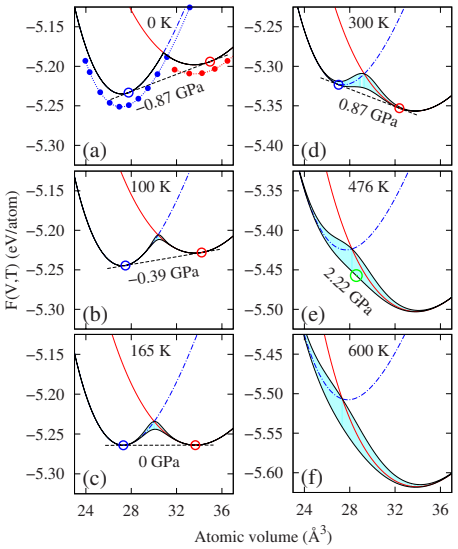

FIG. 4. (Color online). Helmholtz free energies [Eq. (2)] and its components with atomic volume at (a) 0 K; (b) 100 K; (c) 165 K; (d) 300 K; (e) 476 K; and (f) 600 K. Blue (dot-dashed, obscured by the black solid line on the left-hand side) curves: F^{NM} (V,T); red (solid, obscured by the black solid line on the right-hand side) curves: F^{Mag} (V,T); black solid curves on the upper boundaries of the cyan shadows in Figs. 4(b)–4(f) are $\Sigma_\sigma x^\sigma F^\sigma(V,T)$; cyan shadows represent $-TS_{\text{conf}}$; solid black curves on the lower boundary of the cyan shadow in Figs. 4(b)–4(f) are $F(V,T)$, and ○ in Fig. 4(e) is the critical point. The numbers below the black dashed curves [the common tangents between the α-Ce (○, blue circle on the lower volume side) and γ-Ce (○, red circle on the higher volume side)] mark the transition pressure. The 0-K total (static) energies of the nonmagnetic electronic state (lower volume side) and the magnetic electronic state (higher volume side) are plotted in Fig. 4(a) using the solid circles (selected values from DFT) with dotted lines.

B. Free-energy and configurational entropy

Prediction of a double tangent along the free energy curve as a function of volume at low temperature and its disappearance at sufficient temperatures are two prerequisites for any model of the γ–α transition in Ce.[4,15,16] This section will show that our theoretical model suffices well for this purpose. Figure 4 shows our calculated temperature evolution of the Helmholtz free energy in terms of: $F(V,T)$, which is the left-hand side of Eq. (2), shown as the solid black curves just below the cyan shadow in Figs. 4(b)–4(f); $F^{NM}(V,T)$, which is the contribution to $F(V,T)$ from the σ=nonmagnetic state in the right-hand side of Eq. (2), shown as the dot-dashed blue curves; $F^{\text{Mag}}(V,T)$, which is the contribution to $F(V,T)$ from the σ=magnetic state in the right-hand side of Eq. (2), shown as the solid red curves; $\Sigma_\sigma x^\sigma F^\sigma(V,T)$, which is the combined contribution to $F(V,T)$ from both $F^{NM}(V,T)$ and $F^{\text{Mag}}(V,T)$, shown as the solid black curves just above the cyan shadows; and $-TS_{\text{conf}}$, which is the contribution to $F(V,T)$ from the configurational entropy, shown as the cyan

shadows. Each cyan shadow is bounded at higher energies by $\Sigma_\sigma x^\sigma F^\sigma(V,T)$, and at lower energies by $F(V,T)$. Note that the transition pressure is the slope of the common tangent denoted by the dashed black line running through the open (blue and red) circles. The six plots in Fig. 4 correspond to: 0 K [Fig. 4(a)]; 100 K below the 0-GPa phase transition [Fig. 4(b)]; 165 K at the 0-GPa phase transition point [Fig. 4(c)]; 300 K [Fig. 4(d)], 476 K [the critical point, Fig. 4(e)], and 600 K [above the critical point, Fig. 4(f)].

The dotted blue (lower volume side) and red (higher volume side) dotted curves in Fig. 4(a) correspond to the 0-K total (static) nonmagnetic and magnetic energies, respectively. Selected points computed from DFT are indicated by the solid blue (lower volume side) and red (higher volume side) circles. The minimum along the 0-K total (static) energy curve for the nonmagnetic electronic state (lower volume side) is at 27.1 Å^3, which is near the 77-K experimental α-Ce atomic volume[3] of 28.5 Å^3. The minimum along the 0-K total (static) energy curve for the magnetic electronic state (higher volume side) is at 33.5 Å^3 (spin moment$=\sim 1.1$). This is close to the 298-K experimental γ-Ce atomic volume[3] of 34.367 Å^3. Note that the free energies (solid curves) are higher than the static energies (dotted curves) due to the zero point energy contribution. Figure 4(b) shows that the nonmagnetic electronic state has a lower free energy minimum than that of the magnetic electronic state at 100 K, suggesting stability of α-Ce at zero pressure. Note that the small cyan shadow near the intersection of the blue (dot-dashed) and red (solid) curves denotes a small nonzero value of $-TS_{\rm conf}$ at 100 K. As temperature increases, $F^{\rm Mag}(V,T)$ decreases faster than $F^{NM}(V,T)$ since the magnetic electronic state has a higher entropy than the nonmagnetic electronic state. Figure 4(c) shows that at 0 GPa the α–γ transition occurs at 165 K (cf. 141 ± 10 K at 10^{-4} GPa from experiment).[3] For $T>165$ K, Figs. 4(d)–4(f) show that the system is predominantly magnetic Ce and pressure must be applied for the transition to occur. However, at all temperatures a sudden transition of first order with a finite volume collapse would occur if we only compare $F^{NM}(V,T)$ and $F^{\rm Mag}(V,T)$. This was also noted in previous models.[8,9,15] The term $-TS_{\rm conf}$ therefore plays a key role in dictating the critical behavior of the transition. Specifically, Figs. 4(e) and 4(f) [with the critical point denoted by the open circle in Fig. 4(e)] show that at 476 K and above, the double wells merge into a single well denoted by $F(V,T)$ from Eq. (2) (the lower solid black curve) in those plots. Our model therefore suggests that 476 K is a tricritical point.

C. $T\Delta S$, ΔE, and $P\Delta V$ along the phase boundary

Along the $\alpha-\gamma$ phase boundary, $\Delta E=-P\Delta V+T\Delta S$,[16] where ΔE, $P\Delta V$, and $T\Delta S$ represent the changes of the internal energy term, pressure term, and entropy term, respectively. Figure 5 is a plot comparing the predictions from the present theoretical model with experimental data.[18,23] The present model overestimates the entropy change, ΔS (dashed green curve). As discussed in the above section, the overestimate is due to the usage of Eq. (5), which overestimates magnetic entropy. However, this overestimate is compensated by our overestimate of the internal energy term, ΔE (red solid curve), as we only consider the ferromagnetic electronic state for the magnetic phase of Ce. A complete consideration of the magnetic phase should also include other magnetic configurations, such as the ferrimagnetic and antiferromagnetic electronic states,[26] and we surmise that closer accord with experiment would be found in a suitably adjusted version of Fig. 5. Hence, $P\Delta V$, the negative value of which is the driving force for the phase transition ($\Delta F=-P\Delta V$), compares favorably with experiment only when the ferromagnetic electronic state of Ce is considered.

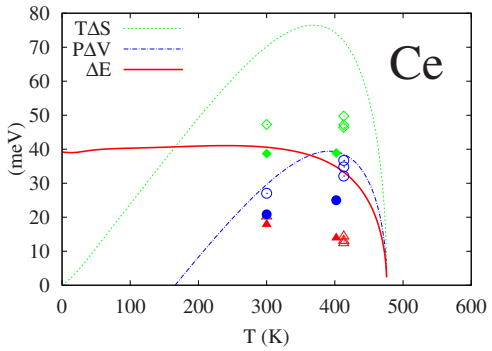

FIG. 5. (Color online). Calculated changes in the entropy term, $T\Delta S$ (green dashed curve), internal energy term, ΔE (red solid curve), and pressure term, $P\Delta V$ (blue dot-dashed curve) along the phase boundary. Open diamonds, circles, and triangles represent, respectively, the measured $T\Delta S$, ΔE, and $P\Delta V$ by Schiwek *et al.* (Ref. 23). Solid diamonds, circles, and triangles represent, respectively, the measured $T\Delta S$, ΔE, and $P\Delta V$ by Beecroft and Swenson (Ref. 18).

D. Fraction of magnetic Ce along the phase boundary

As indicated in the discussion of Eqs. (2) and (3), calculation of the fraction of an individual electronic state in the mixed system is straightforward. Figure 6 shows the fraction $x^{\rm mag}(\gamma)$ of magnetic Ce in α-Ce (blue dot-dashed) and γ-Ce

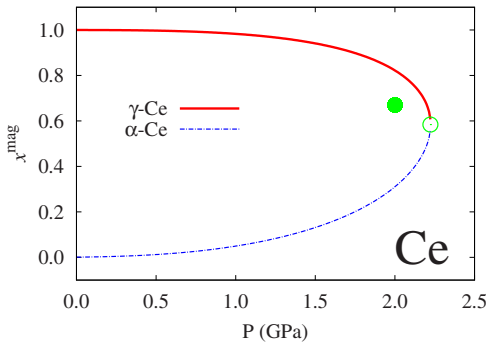

FIG. 6. (Color online). Fraction of magnetic Ce in α-Ce and γ-Ce along the γ–α phase boundary. Red (solid) curve: the calculated $x^{\rm mag}(\gamma)$ (fraction of the magnetic Ce for γ-Ce); blue (dot-dashed) curve, the calculated $x^{\rm mag}(\alpha)$ (fraction of the magnetic Ce for α-Ce); ○, the calculated critical point; and ●, the experimentally estimated critical point [see Svane (Ref. 9) and Koskenmaki and Gschneidner (Ref. 3)].

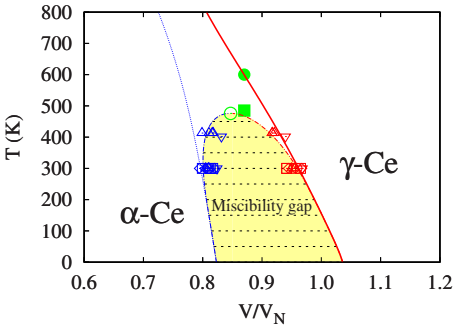

FIG. 7. (Color online). T-V phase diagram of Ce. The blue (dot-dashed) and red (dot-dashed) looping branches denote α-Ce (lower volume side) and γ-Ce (higher volume side), respectively. ○ represents the predicted critical point from the present work. The black dashed lines in the miscibility gap reference values of the volume collapse at T. The blue dotted (red solid) nonmagnetic (magnetic) lines denote the calculated V's at the transition using only the free energies in Eq. (1) for the two Ce states. The experimental data are due to Schiwek *et al.* (Ref. 23) (△ and △); Jeong *et al.* (Ref. 25) (○ and ○); Olsen *et al.* (Ref. 22) (□ and □); Zachariasen and Ellinger (Ref. 20) (◇ and ◇); Beecroft and Swenson (Ref. 18) (▽ and ▽); Schiwek *et al.* (Ref. 23) (■); and Koskenmaki and Gschneidner (Ref. 3) (●).

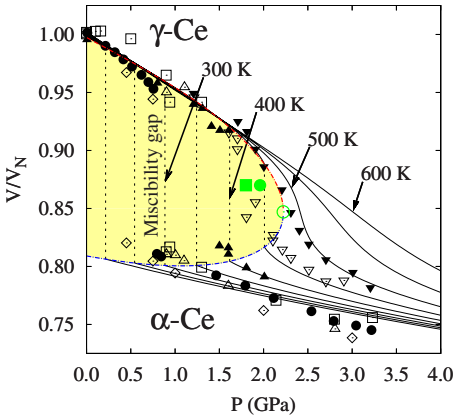

FIG. 8. (Color online). Equation of states for Ce. The black solid lines represent the calculated isotherms from 200 to 600 K at $\Delta T = 50$ K increments. ○ is our calculated critical point. The blue and red dot-dashed lines correspond to α-Ce (lower volume side) and γ-Ce (higher volume side), respectively. The region delimited by these two branches consists of the double phase region (or miscibility gap) with the vertical dashed lines [derived by means of Maxwell's "equal area rule" (Refs. 5 and 27)] denoting the equilibrium P at T. Experimental data are due to Olsen *et al.* (Ref. 22) (◇: 300 K); Jeong *et al.* (Ref. 25) (●: 300 K); Zachariasen and Ellinger (Ref. 20) (□: 300 K); Schiwek *et al.* (Ref. 23) (△: 300 K; ▲: 413 K; ▽: 493 K; ▼: 573 K; big green ■: 485 K, critical point); and Koskenmaki and Gschneidner (Ref. 3) (big green ●: 600 K, critical point).

(red solid) with P along the phase boundary estimated using $x^{\sigma}=Z^{\sigma}/Z$. We note that the fraction of the magnetic electronic state in α-Ce increases with increasing pressure while the fraction of the magnetic electronic state in γ-Ce decreases. At the critical point (open circle in Fig. 6), the fraction of magnetic Ce is calculated to be 0.58. This is in qualitative agreement with the 0.67 value (filled circle in Fig. 6) estimated experimentally at the critical point (see Svane[9] and Koskenmaki and Gschneidner[3]).

E. T-V phase diagram

Figure 7 shows the calculated T-V phase diagram compared with data from a variety of experiments.[3,20,22,23,25] The calculated phase boundary is illustrated by the blue and red dot-dashed looping branches in Fig. 7 denoting α-Ce (lower volume side) and γ-Ce (higher volume side), respectively, which enclose the miscibility gap (yellow shadow). The dashed horizontal lines (so-called tie lines[56]) in the miscibility gap denote calculated values of the volume collapse, $V_{\gamma}-V_{\alpha}$, at the associated value of T. The calculated critical point is denoted by the open green circle. We note that the experimental data included in the plot (open up-triangles,[23] down-triangles,[18] circles,[25] and squares[22] for the phase boundary, and the solid green circle[3] and square[23] for the critical point) are generally in close agreement with our predicted T-V phase diagram. To investigate the role of S_{conf}, we have also computed the phase transition using only $F^{NM}(V,T)$ and $F^{\text{Mag}}(V,T)$. The results are also plotted in Fig. 7. If S_{conf} is neglected, then the calculated phase boundary curves for α-Ce and γ-Ce never cross one another as indicated by the blue (dotted) and red (solid) lines. Hence, without $-TS_{\text{conf}}$, no critical point is predicted within 0–800 K. The effects of configurational entropy, S_{conf}, were noted by Johansson *et al.*[8] and in subsequent work[9,15] but not with the detail shown in Fig. 7.

F. Equation of states

The EOS for the Ce transition has previously been computed up to the critical temperature.[5,9,10,15] However, no comparisons of relevant experimental data with prior EOS predictions over the temperature range of relevance to the Ce transition have been reported. Figure 8 compares our computed EOS with a collection of experimental data.[3,20,22,23,25] The relative volume as V/V_N from 200 to 600 K at 50-K increments is plotted as the black solid lines. Symbols denoting experimental data in Fig. 8 are associated with the same experimental references as those in Fig. 7. In particular, experimental data follow our computed isotherms in Fig. 8 very closely. For V/V_N vs P within the phase change region, the $\gamma \rightarrow \alpha$ volume collapse is again noted, with the magnitude of the collapse increasing with decreasing T. This is shown explicitly by the dashed vertical lines at $T=200$, 250, 300, 350, 400, and 450 K. For V/V_N vs P at $T>476$ K, the calculated isotherms show an anomalous slope change, which closely matches the behavior near $V/V_N=\sim 0.85$ from experiment.[23]

VII. Summary

Starting with a partition function, we have developed a complete thermodynamic description of the γ–α isostructural phase transition in Ce wherein all inputs are provided

by first-principles DFT calculations. We have quantitatively addressed the mixing of nonmagnetic and magnetic Ce $4f$ states at finite temperatures. This provides the correct phase transition thermodynamics as demonstrated in our computed free energy curves from 0 to 600 K, and temperature-volume phase diagram. Important physical quantities that characterize the γ–α isostructural phase transition, such as the critical point, phase transition temperature at ambient pressure, $\gamma \rightarrow \alpha$ volume collapse, and $P\Delta V$, are predicted to be in remarkably good agreement with available experimental data. We demonstrate the important role of the configurational mixing entropy in leading to the critical behavior of the transition. Our approach is unique from the standpoint that vibrational free energies are computed with phonon theory based upon the direct method of lattice dynamics for both nonmagnetic and magnetic Ce $4f$ states. We note that the approach developed herein is readily applicable to the prediction of thermodynamic properties of other strongly correlated materials such as plutonium.

ACKNOWLEDGMENTS

Calculations were conducted at the General Motors High Performance Computing Center and the LION clusters at the Pennsylvania State University (supported in part by National Science Foundation Grants No. DMR-9983532, No. DMR-0122638, and No. DMR-0205232, and in part by the Materials Simulation Center and the Graduate Education and Research Services at the Pennsylvania State University). Additional funding from the National Science Foundation through Grants No. DMR-0510180 and No. DMR-0205232 is gratefully acknowledged. L. G. Hector, Jr. acknowledges the kind assistance of P. Saxe and E. Wimmer.

[1] P. Ward and D. Brownless, *Rare Earth: Why Complex Life is Uncommon in the Universe* (Springer, New York, 2000).
[2] P. W. Bridgman, Proc. Am. Acad. Arts Sci. **62**, 207 (1927).
[3] D. C. Koskenmaki and K. A. Gschneidner, in *Handbook on the Physics and Chemistry of the Rare Earths*, edited by K. A. Gschneidner and L. Eyring (North-Holland, Amsterdam, 1978), Vol. 1, p. 337.
[4] J. W. Allen and R. M. Martin, Phys. Rev. Lett. **49**, 1106 (1982).
[5] J. W. Allen and L. Z. Liu, Phys. Rev. B **46**, 5047 (1992).
[6] A. Svane, Phys. Rev. Lett. **72**, 1248 (1994).
[7] Z. Szotek, W. M. Temmerman, and H. Winter, Phys. Rev. Lett. **72**, 1244 (1994).
[8] B. Johansson, I. A. Abrikosov, M. Alden, A. V. Ruban, and H. L. Skriver, Phys. Rev. Lett. **74**, 2335 (1995).
[9] A. Svane, Phys. Rev. B **53**, 4275 (1996).
[10] J. Laegsgaard and A. Svane, Phys. Rev. B **59**, 3450 (1999).
[11] Y. Wang, Phys. Rev. B **61**, R11863 (2000).
[12] K. Held, A. K. McMahan, and R. T. Scalettar, Phys. Rev. Lett. **87**, 276404 (2001).
[13] A. K. McMahan, K. Held, and R. T. Scalettar, Phys. Rev. B **67**, 075108 (2003).
[14] L. de' Medici, A. Georges, G. Kotliar, and S. Biermann, Phys. Rev. Lett. **95**, 066402 (2005).
[15] M. Lüders, A. Ernst, M. Däne, Z. Szotek, A. Svane, D. Ködderitzsch, W. Hergert, B. L. Györffy, and W. M. Temmerman, Phys. Rev. B **71**, 205109 (2005).
[16] B. Amadon, S. Biermann, A. Georges, and F. Aryasetiawan, Phys. Rev. Lett. **96**, 066402 (2006).
[17] B. Johansson, Philos. Mag. **30**, 469 (1974).
[18] R. I. Beecroft and C. A. Swenson, J. Phys. Chem. Solids **15**, 234 (1960).
[19] A. Jayaraman, Phys. Rev. **137**, A179 (1965).
[20] W. H. Zachariasen and F. H. Ellinger, Acta Crystallogr., Sect. A: Cryst. Phys., Diffr., Theor. Gen. Crystallogr. **33**, 155 (1977).
[21] A. R. Kutsar, Sov. Phys. Dokl. **24**, 292 (1979).
[22] J. S. Olsen, L. Gerward, U. Benedict, and J. P. Itie, Physica B & C **133**, 129 (1985).
[23] A. Schiwek, F. Porsch, and W. B. Holzapfel, High Press. Res. **22**, 407 (2002).
[24] W. Kohn and L. Sham, Phys. Rev. **140**, A1133 (1965).
[25] I. K. Jeong, T. W. Darling, M. J. Graf, T. Proffen, R. H. Heffner, Y. Lee, T. Vogt, and J. D. Jorgensen, Phys. Rev. Lett. **92**, 105702 (2004).
[26] C. Kittel, *Introduction to Solid State Physics* (Wiley, Hoboken, NJ, 2005).
[27] L. D. Landau and E. M. Lifshitz, *Statistical Physics* (Pergamon, Oxford, 1980-1981).
[28] G. Kresse and J. Hafner, Phys. Rev. B **49**, 14251 (1994).
[29] G. Kresse and J. Furthmüller, Comput. Mater. Sci. **6**, 15 (1996).
[30] G. Kresse, http://cms.mpi.univie.ac.at/vasp/vasp/vasp.html
[31] P. E. Blöchl, Phys. Rev. B **50**, 17953 (1994).
[32] G. Kresse and D. Joubert, Phys. Rev. B **59**, 1758 (1999).
[33] J. P. Perdew, K. Burke, and M. Ernzerhof, Phys. Rev. Lett. **77**, 3865 (1996).
[34] K. Parlinski, J. Phys.: Conf. Ser. **92**, 012009 (2007).
[35] K. Parlinski, Z. Q. Li, and Y. Kawazoe, Phys. Rev. Lett. **78**, 4063 (1997).
[36] S. Baroni, S. de Gironcoli, A. Dal Corso, and P. Giannozzi, Rev. Mod. Phys. **73**, 515 (2001).
[37] K. Parlinski, J. Lazewski, and Y. Kawazoe, J. Phys. Chem. Solids **61**, 87 (2000).
[38] M. Methfessel and A. T. Paxton, Phys. Rev. B **40**, 3616 (1989).
[39] L. G. Hector, Jr., J. F. Herbst, W. Wolf, P. Saxe, and G. Kresse, Phys. Rev. B **76**, 014121 (2007).
[40] A. P. Murani, S. J. Levett, and J. W. Taylor, Phys. Rev. Lett. **95**, 256403 (2005).
[41] M. B. Zolfl, I. A. Nekrasov, T. Pruschke, V. I. Anisimov, and J. Keller, Phys. Rev. Lett. **87**, 276403 (2001).
[42] S. L. Dudarev, L. M. Peng, S. Y. Savrasov, and J. M. Zuo, Phys. Rev. B **61**, 2506 (2000).
[43] A. Rohrbach, J. Hafner, and G. Kresse, Phys. Rev. B **69**, 075413 (2004).
[44] H. W. Sheng, H. Z. Liu, Y. Q. Cheng, J. Wen, P. L. Lee, W. K. Luo, S. D. Shastri, and E. Ma, Nat. Mater. **6**, 192 (2007).
[45] M. Petersen, J. Hafner, and M. Marsman, J. Phys.: Condens. Matter **18**, 7021 (2006).

[46] A. Rohrbach, J. Hafner, and G. Kresse, J. Phys.: Condens. Matter **15**, 979 (2003).
[47] A. van de Walle and G. Ceder, Rev. Mod. Phys. **74**, 11 (2002).
[48] G. Kresse, J. Furthmüller, and J. Hafner, Europhys. Lett. **32**, 729 (1995).
[49] A. B. Alchagirov, J. P. Perdew, J. C. Boettger, R. C. Albers, and C. Fiolhais, Phys. Rev. B **63**, 224115 (2001).
[50] J. W. van der Eb, Ph.D. thesis, University of Groningen, 2000.
[51] K. Haule, V. Oudovenko, S. Y. Savrasov, and G. Kotliar, Phys. Rev. Lett. **94**, 036401 (2005).
[52] M. E. Manley, R. J. McQueeney, B. Fultz, R. Osborn, G. H. Kwei, and P. D. Bogdanoff, Phys. Rev. B **65**, 144111 (2002).
[53] C. Stassis, T. Gould, O. D. McMasters, K. A. Gschneidner, and R. M. Nicklow, Phys. Rev. B **19**, 5746 (1979).
[54] M. E. Manley, R. J. McQueeney, B. Fultz, T. Swan-Wood, O. Delaire, E. A. Goremychkin, J. C. Cooley, W. L. Hults, J. C. Lashley, R. Osborn, and J. L. Smith, Phys. Rev. B **67**, 014103 (2003).
[55] I. Barin, *Thermochemical Data of Pure Substances* (Wiley-VCH Verlag, Weinheim, 1995).
[56] M. Hillert, *Phase Equilibria, Phase Diagrams and Phase Transformations: Their Thermodynamic Basis* (Cambridge University Press, Cambridge, England, 1998).